A comparison of single-reed and bowed-string excitations of a hybrid wind instrument

Conference or Workshop Item

A COMPARISON OF SINGLE-REED AND BOWED-STRING EXCITATIONS OF A HYBRID WIND INSTRUMENT

Kurijn Buys, David Sharp, and Robin Laney

Faculty of Mathematics Computing and Technology,
The Open University, Milton Keynes, UK
Kurijn.Buys@open.ac.uk

ABSTRACT

A hybrid wind instrument is constructed by connecting a theoretical excitation model (such as a real-time computed physical model of a single-reed mouthpiece) to a loudspeaker and a microphone which are placed at the entrance of a wind instrument resonator (a clarinet-like tube in our case). The successful construction of a hybrid wind instrument, and the evaluation with a single-reed physical model, has been demonstrated in previous work [1, 2]. In the present paper, inspired by the analogy between the principal oscillation mechanisms of wind instruments and bowed string instruments, we introduce the stick-slip mechanism of a bow-string interaction model (the hyperbolic model with absorbed torsional waves) to the hybrid wind instrument set-up. Firstly, a dimensionless and reduced parameter form of this model is proposed, which reveals the (dis-)similarities with the single-reed model. Just as with the single-reed model, the hybrid sounds generated with the bow-string interaction model are close to the sounds predicted by a complete simulation of the instrument. However, the hybrid instrument is more easily destabilised for high bowing forces. The bow-string interaction model leads to the production of some raucous sounds (characteristic to bowed-string instruments, for low bowing speeds) which represents the main perceived timbral difference between it and the single-reed model. Another apparent timbral difference is the odd/even harmonics ratio, which spans a larger range for the single-reed model. Nevertheless, for both models most sound descriptors are found within the same range for a (stable) variety of input parameters so that the differences in timbre remain relatively low. This is supported by the similarity of both excitation models and by empirical tests with other, more dynamic excitation models.

1. INTRODUCTION

The development and early evaluation of a hybrid wind instrument using a loudspeaker has been described in earlier work [1, 2]. Figure 1 explains the concept: a physical "excitation model" (for instance a single-reed embouchure) is simulated on a computer and interacts with a real acoustical resonator so that the whole is able to generate hybrid self-sustained sounds.

Such a device supports two main research interests. First, placing it in the context of acoustic wind instrument research, it would be of substantial value to have a repeatable and precisely quantified control over an exciter that is linked to a resonator of interest. This matches with the objectives of the now well-established "artificial mouths" for wind instruments (e.g. [3]). A second interest, is the exploration of the device's potential as a musical instrument, mostly from the timbre perspective, which is an active musical focus of today. Here, the same control precision can play a role in the accessibility of certain (variations of) sounds. While, the computed environment allows

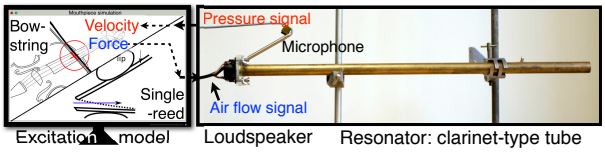

Figure 1: The hybrid wind instrument set-up: a computed excitation model (a single-reed embouchure model or a bow-string interaction model) in interaction with a physical resonator by means of a loudspeaker and a microphone.

modeling any conceivable excitation and handles electronic parameter variations, the physical control over the resonator (the fingering) remains, which opens up an alternative range of musical expression with the advantage of relatively low computational power needs.

Only minor contributions on the hybrid wind instrument concept have been made to date. Maganza first briefly explored a set-up [4] and since then a small number of works on closely related subjects have been carried out, for example [5, 6, 7]. More recently, an identical approach has been implemented, but using an electrovalve as flow actuator [8]. For our hybrid instrument, a loudspeaker is used to perform the actuation and it has been shown that, by introducing some correcting filters, a very good accuracy can be achieved, so that realistic clarinet tones can be produced [1, 2]. The hybrid instrument set-up is briefly reviewed in section 2.

Given the similar fundamental oscillation principle of wind and bowed string instruments [9], the pressure and air-flow at the resonator entrance can be interpreted by the computer as respectively a string velocity and force, so that the stick-slip mechanism of a bow-string interaction model (hereafter referred to as a BS model) can be introduced to the hybrid wind instrument set-up. This idea is of particular musical interest, since such a physically impossible combination can potentially lead to uncommon timbres.

In the present paper, we compare the quasi-static single-reed embouchure model (hereafter referred to as the SR model) and a BS model and their evaluation with the hybrid wind instrument. While an earlier study by Ollivier et al. [10] has discussed the analogy between woodwinds and the bowed string, their BS model was based on a mathematical simplification of the hyperbolic model [9] whose parameters have a poor connection to the physical reality. This model was initially introduced by Weinreich and used later by Müller for their hybrid string instruments [11, 12]. In our study, we propose a dimensionless and reduced parameter form of the original hyperbolic BS model.

After the presentation of the SR and BS models in section 3, in section 4 a theory for the estimation of sound features is

proposed and applied for those excitation models. In section 5 both excitation models are evaluated with the hybrid instrument and with an entire simulation.

We note that, for simplicity, the t argument for time domain signals is not repeated after the introduction of a variable.

2. PRESENTATION OF THE HYBRID WIND INSTRUMENT

Preliminary work has been carried out to investigate the behaviour of a loudspeaker mounted on a tube [1, 2, 13] (see those papers for a detailed explanation).
As the loudspeaker doesn't provide an ideal rigid termination to the tube, coupled physical models of the loudspeaker and tube are considered. Also, measurements are performed to find the parameter values that are used both to predict a calibrated "flow rate response" for the loudspeaker and to account for the coupling. For coherent functioning of the hybrid instrument, the calculated flow rate signal by the excitation model should be acoustically reproduced by the loudspeaker as a physical air flow. Therefore, two filters are considered: a feedforward filter, to flatten the loudspeaker response and a feedback filter, to account for the coupling with the tube. These filters are executed by the real-time computing system[1] that is also used to execute the excitation models. The resonator is a clarinet-like tube with an inner diameter of 14.2 mm, a length of 58 cm and entrance impedance $Z_t = \frac{P}{Q}$ (where P and Q are the Fourier transform of respectively the pressure $p(t)$ and air flow rate $q(t)$ at the resonator entrance). Its first resonance frequency is found at 139.8 Hz while, for example, the fifth resonance lies at 1275.3 Hz. This is 17.2 Hz higher than the integer multiple of the first resonance, which attests for a positive inharmonicity.

2.1. Accounting for the loudspeaker

Figure 2 depicts a schematic diagram of the implemented feedforward- and feedback filters to account for the presence of the loudspeaker (we used a 1 " Tang Band loudspeaker of type W1-1070SE with an additional mass on the membrane).

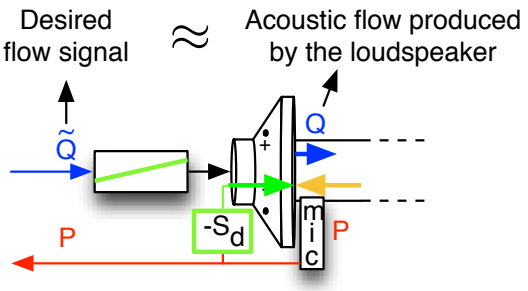

Figure 2: A feedback- and a feedforward filter account for the loudspeaker

Assuming the loudspeaker to be a simple mass-spring-damper system, the feedforward filter that would undo its response would simply be the inverse of the loudspeaker transfer function. The loudspeaker's resonant frequency lies far enough below the playing frequencies so that mainly the inertia is of importance, which can be compensated by a derivative filter. Further, a "lead-lag filter" is also added to compensate for phase deviations near the loudspeaker resonant frequency (for a detailed description, see [13]). The total filter is found to effectively flatten the gain response of the filter-loudspeaker system, while the phase response remains at 0 just after the loudspeaker resonance and then slowly decreases by about $18°\text{kHz}^{-1}$ (which cannot be compensated for).

When the loudspeaker is placed at the entrance of the tube, the strong pressure variations in front of it will impose an important force on the membrane so that those components will be in a coupled interaction. A simple resolution for this issue is based on Newton's third law: in order to undo the force on the loudspeaker diaphragm (with area S_d) due to the pressure p in front of it (measured with a microphone), it is necessary to add an opposite force ($-S_d\ p$) to the electric force generated by the voice coil. This can be done with a feedback filter, by taking into account the voltage-to-force transfer function of the electrical loudspeaker part.

Altogether, the impedance $\widetilde{Z}_{ts} = \frac{\widetilde{Q}}{P}$, measured with a sine-swept signal on the filters-loudspeaker-tube-system (that will be put in interaction with the excitation model), turns out to be fairly close to the original measured tube impedance $Z_t = \frac{Q}{P}$. The zero-crossings of their phase responses, which are an important indicator for potential self-sustained playing frequencies, match reasonably well. Finally it is noted that the increasing phase lag (and another nonlinear side-effect which we will not discuss in the present paper), causes the initially positive inharmonicity in Z_t to become negative in the impedance that is visible to the programmed excitation model.

3. SINGLE-REED AND BOW-STRING EXCITATION MODELS

This section provides a physical description of the excitation models. For the numerical implementation it is important to consider that the physical situation, which is bi-directional in nature, needs to be converted into a looped sequential procedure. This involves converting the presented "implicit equations" into "explicit equations" which exceeds the scope of this paper (however, for the numerical evaluation the explicit equations are used).

3.1. Single-reed embouchure model

For the SR model, we adopted the classical theory from Wilson and Beavers [3] (and further developed in [15]).

3.1.1. Physical model

The reed (including the player's lower lip) is considered to behave as a mass-spring-damper system, driven by the pressure difference across the reed $\Delta p(t) = p_m - p$ (with p_m the mouth pressure and $p(t)$ the pressure inside the mouthpiece), acting on part of the reed surface S_r. Hence, the reed's dynamics are described by:

$$\frac{1}{\omega_r^2}\frac{d^2\,y}{dt^2} + \frac{1}{Q_r\,\omega_r}\frac{d\,y}{dt} + y = \frac{-S_r \Delta p}{k}, \qquad (1)$$

with $y(t)$, the displacement of the reed with stiffness k, resonance frequency ω_r and quality factor Q_r.

The air flow that enters the instrument can be expressed as the product of the flow velocity $v_f(t)$ and the effective reed opening cross-section S_f. The former can be found by the Bernoulli theorem applied between the mouth and the reed flow

[1] In order to fulfill the real-time requirements, we made use of the *Xenomai* framework [14], applied on a standard PC equipped with an acquisition card (with analogue in and outs). A sampling rate of f_s = 40 kHz could be obtained, which is high enough for our purpose.

channel (thus between the mentioned pressure difference) and the latter is assumed to be linearly related to the reed displacement. The resulting flow rate can be expressed as:

$$q = \underbrace{sgn(\Delta p)\sqrt{\frac{2|\Delta p|}{\rho}}}_{v_f}\underbrace{\mathcal{H}(y+H)(y+H)w}_{S_f},$$

where ρ is the air density and w is the effective reed width. The sgn operator is introduced to make the calculation of negative flows possible and the Heaviside function $\mathcal{H}$ to hold a zero flow rate when the reed hits against the lay at position $y = -H$, which occurs above the "beating pressure" P_M .

These equations can be simplified and made dimensionless by defining $\bar{y} = \frac{y}{H}$, $\bar{p} = \frac{p}{P_M}$, $\bar{q} = \frac{q\,Z_c}{P_M}$, $\bar{\Delta p} = \frac{\Delta p}{P_M}$:

$$\begin{cases} \dfrac{1}{\omega_r^2}\dfrac{d^2\,\bar{y}}{dt^2} + \dfrac{1}{Q_r\,\omega_r}\dfrac{d\,\bar{y}}{dt} + \bar{y} = -\Delta p \\ \bar{q} = sgn(\bar{\Delta p})\sqrt{|\bar{\Delta p}|}\zeta\mathcal{H}(\bar{y}+1)(\bar{y}+1), \end{cases} \tag{2}$$

where ζ lumps all remaining embouchure parameters together and its time variation is related to the lip-pressure variation on the reed. We note the dimensionless mouth pressure $\gamma = \frac{p_m}{P_M}$, so that $\bar{\Delta p}(t) = \gamma - \bar{p}$, with $\bar{p}(t)$, the dimensionless mouthpiece pressure.

There are three main remaining independent parameters: P_M, which determines the signal amplitude (without timbre variation within the linear dynamic range of a resonator), the mouth pressure γ and the "embouchure parameter" ζ, which both have an effect on the signal shape and transients, and thus the timbre of the sound. It is further assumed that the mouth pressure remains constant.

Typical parameter ranges for the clarinet are $P_M < 10$kPa, $\zeta \approx [0.1, 0.8]$ and $\gamma \approx [1/3, 2.5]$. The dynamic parameters are of importance to the brightness and to choosing the desired register. The quality factor range is $Q_r = [5, 125]$ and ω_r should be above the frequency of the first harmonic [3].

By separating the dimensionless mouthpiece pressure as pointed out earlier: $\bar{p} = \bar{p}_h + \bar{q}$, eqs. (2) become an implicit relation which can be solved analytically by following a recently proposed solution by Guillemain et al. [16]. We don't develop the discretisation steps here, but the detailed development can be found in [16, 13].

3.2. Bow-string interaction model

3.2.1. Analogy

As McIntyre et al. [9] have pointed out, there are significant common features in the fundamental physical functioning of instruments that produce self-sustained tones. They all consist of a resonator that is coupled to an excitation mechanism, with the resonator and excitation mechanism each imposing a relation between two physical quantities so that the combined set of relations can result in a self-sustained oscillation. As such, the sound production of a single-reed instrument can be compared to that of a bowed-string instrument, the resonator being respectively the vibrating air column and the string (when symmetrical and bowed exactly at its midpoint), the excitation mechanism being the embouchure and the bow-string interaction, and the physical quantities being the pressure-air flow-rate coupling and the bow/string velocity-force coupling.

This analogy inspired the idea of combining the BS mechanism with an acoustic resonator. The computer allows a pressure and flow rate signal to be interpreted as if it were respectively a velocity and force between a bow and a string, so that the concept can be realised on a hybrid instrument. Knowing that the more detailed functioning of both instruments differs and is responsible for their characteristic sounds, it can be anticipated that such a combination will produce a sound that contains a mixture of characteristics of the wind and bowed-string instrument.

3.2.2. Physical model

In contrast to the SR case, several BS models are currently in common usage, which is probably due to the empirical persistence of elementary models that allow mathematical simplicity [2]. For this reason of simplicity, it was initially decided to employ the "hyperbolic model", which draws from the stick-slip mechanism. In this model, during the "sticking phase", the velocity difference between bow and string surface $\Delta v'(t)$ remains zero until the force $f(t)$ between those parts reaches a break-away sticktion force $f_b\mu_s$. During the "slipping phase", Coulomb (viscous-less) friction with the Stribeck effect occurs as long as the bow and string differ in velocity. This is modeled by the following set of equations:

$$\begin{cases} & \text{as long as:} \\ f = sgn(\Delta v')f_b(\mu_d + \frac{(\mu_s-\mu_d)v_0}{|\Delta v'|+v_0}) & \Delta v' \neq 0 \\ \Delta v' = 0 & f < f_b\mu_s \end{cases} \tag{3}$$

It has been reported that the quality of simulations significantly improves by including the string rotations in this model[9]. By defining $\Delta v(t) = v_b - v(t)$ as the difference between the bow and the string axis, the previous velocity difference can be expressed as :

$$\Delta v' = \Delta v - \frac{f}{2Z_R}, \tag{4}$$

where Z_R is the characteristic impedance for torsional waves. Note that these waves are assumed to be completely absorbed so that no reflections are considered.

3.2.3. A dimensionless and reduced parameter form

Just as for the SR model, it is possible to rewrite the equations of this BS model in terms of dimensionless quantities and with a reduced set of independent input parameters. By introducing the dimensionless force $\bar{f} = \frac{f}{2Z_c v_0}$ and velocity $\bar{\Delta v} = \frac{\Delta v}{v_0}$ and using eq.(4), eqs. (3) can be rewritten as:

$$\bar{f} = \begin{cases} & \text{as long as:} \\ sgn(\bar{\Delta v})\zeta_b(\delta + \frac{1-\delta}{|\bar{\Delta v} - \alpha\bar{f}|+1}) & |\bar{\Delta v}| > \alpha\zeta_b \\ \frac{\bar{\Delta v}}{\alpha} & |\bar{\Delta v}| \leq \alpha\zeta_b, \end{cases} \tag{5}$$

where $\zeta_b = \bar{f}_b\mu_s = \frac{f_b\mu_s}{2Z_c v_0}$, $\delta = \frac{\mu_d}{\mu_s}$ and $\alpha = \frac{Z_c}{Z_R}$. This form shows that the parameter v_0 is solely controlling the amplitude of the oscillations (for a bowing force proportionally varying with v_0, i.e. for a constant $\bar{f}_b$). Due to the fact that μ_s and $\bar{f}_b$ play the same role (for constant δ), these parameters are merged into a global bow-force related parameter ζ_b (chosen in analogy to the embouchure parameter ζ). While there is still an $\alpha\bar{f}$ term in the equation of the slipping branch, it is small enough compared with $\bar{\Delta v}$ for typical BS parameters that ζ_b is almost directly proportionally controlling the excitation amplitude of that curve. Also in analogy with the SR model, we introduce the dimensionless bowing velocity $\gamma_b = \frac{v_b}{v_0}$, so that $\bar{\Delta v}$=$\gamma_b - \bar{v}$,

[2] e.g. a recent more advanced model takes into account the thermal effects of rosin [17]

where $\bar{v} = \frac{v}{v_0}$ is the dimensionless velocity of the string axis. Typical parameter values are $v_0 \approx 0.2$ m/s, $\delta \approx [3/8, 2/4]$, $\alpha \approx [0.26, 1]$, $\zeta_b \approx \frac{[10,50]}{\mathrm{N}} f_b$, with $f_b \approx [0.15, 3]$N and $\gamma_b \approx (5\,\mathrm{s/m})\, v_b$ with $v_b \approx [0.04, 3]$m/s [18, 19, 9]. However, these bow force and velocity ranges are based on low bow-bridge distances; much lighter forces (or higher bow velocities) are required when the middle of the string is bowed [9].
For the numerical simulation, an explicit analytical expression is obtained in a similar manner as for the SR model (a detailed description will be published later).

4. EXCITATION MODELS VS. SOUND FEATURES

In this section, the issue of how the interaction of the excitation models and the resonator determine the sounds produced is discussed. Understanding this relationship allows us to pre-estimate the sound features, providing a tool to select excitation models and/or parameters as a function of a desired sound output.

We consider the excitation models to be non-dynamic in nature here. The SR model's reed resonance frequency and Q factor are considered (and programmed) high enough so that the model may assumed to be quasi-static and only the non-hysteretic case of the BS model is considered (the hysteretic case requires high ζ_b values which result in the appearance of parasitic noises with the hybrid instrument.)

In this section we mainly refer to the SR case, but the theory also applies to the BS case (by replacing q by f and p by v). Also, from here onwards, $\gamma_{(b)}$ and $\zeta_{(b)}$ refer to each of the relevant SR and BS parameters. That is, $\gamma_{(b)}$ refers to both γ and γ_b, while $\zeta_{(b)}$ refers to both ζ and ζ_b.

4.1. Oscillation conditions and amplitude

In order for an oscillation to occur, the excitation should provide a positive energy contribution that sufficiently compensates for the acoustic losses. Hence, for given excitation parameters, the nonlinear function should have a minimal rise (also known as a "negative resistance") at $p = 0$, i.e. $\bar{q}'(\bar{p} = 0) > 1 - \lambda \gtrsim 0$, where $\lambda (< 1)$ is a real constant that represents the frequency independent losses of the acoustic resonator. [3].

First we consider how a new nonlinear function can be obtained, which includes the resonator's frequency independent losses λ [20]. This theory states that an equivalent system can be obtained, consisting of a resonator without the frequency independent losses and a new nonlinear curve $\tilde{\bar{q}}(\bar{p})$ corresponding to $\bar{q}(\bar{p})$ stretched away by a factor $\frac{1}{\lambda}$ from a line that crosses the $\{\bar{p}, \bar{q}\}$ origin at 45°. Both of these curves, and the mirrored $\tilde{\bar{q}}$ and $\tilde{\bar{f}}$ curves, are depicted (for $\{\zeta = 0.2, \gamma = 0.8\}$, $\{\zeta_b = 0.6, \gamma_b = 1\}$ and $\lambda = 0.94$) in figure 3 for the SR model and figure 4 for the BS model.

It can be shown (e.g. using an iterative approach as in [20]) that a (stable) oscillation requires three intersections between the new nonlinear curve and its mirrored counterpart. The amplitude will settle at the outer intersections, which increases for increasing $\gamma_{(b)}$ (becoming linear, until near the oscillation's extinction when the intersection jumps to one point again).

4.2. Brightness

To explain the spectral development as a function of the excitation model's parameters, we need to consider how the remaining, frequency dependent, acoustic losses intervene. These losses introduce a dispersion that will enforce high frequencies to decrease in amplitude. On the other hand, the nonlinear characteristic excitation curve has the potential to re-introduce high frequencies so that finally the oscillation will settle on a balanced amount of high frequencies. Given that the resonator accentuates odd harmonics, and given that it is the anti-symmetrical component of the excitation curve (which is an "odd function") that is responsible for the introduction of odd harmonics, one can understand that the amount of asymmetry will be an indicator of the "spectral compensation". [4]. This function can be obtained by $\tilde{\bar{q}}_o = \frac{\tilde{\bar{q}}(\bar{p}) - \tilde{\bar{q}}(-\bar{p})}{2}$, which is also depicted in figure 3 and $\tilde{\bar{f}}_o$ in figure 4.
Given that this "spectral compensation rule" applies over the entire evaluated pressure domain of the nonlinear function, and that a precise study of the spectral turnout would be complicated, we make the empirical assumption that the mean absolute amplitude of this curve $< |\tilde{\bar{q}}_o| >$ (later referred to as the "odd amplitude") is positively compensating and thus acts as a global indicator of the relative spectral richness or "brightness" [5]. Therefore it is interesting to study the evolution of this odd amplitude for various excitation parameter ranges. The $\gamma_{(b)}$ values used in figures 3 and 4 result in maximal odd amplitudes (indicated by the blue shaded area). Above and below these mouth pressures and bow velocities these amplitudes decrease, as can

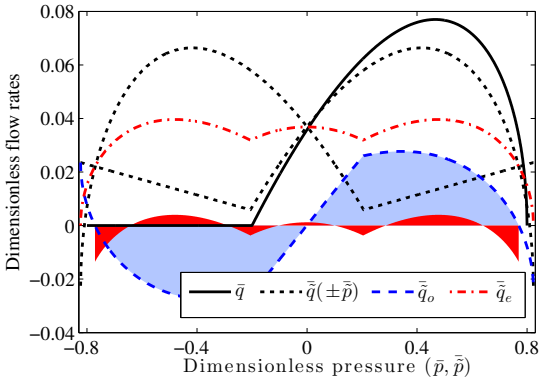

Figure 3: Characteristic nonlinear curves for the SR model

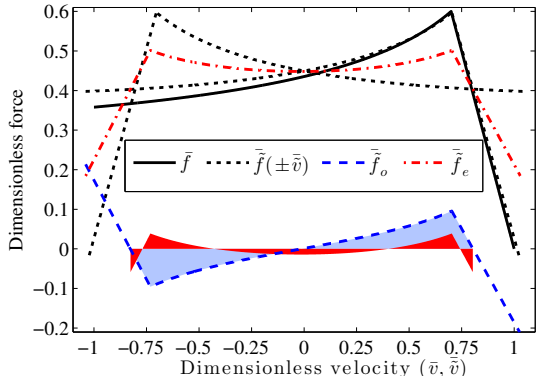

Figure 4: Characteristic nonlinear curves for the BS model.

[3] For a cylindrical open tube with no radiation at the open end, so that losses only occur inside the tube, $\lambda = \exp(-2\alpha_a l)$, where α_a is the absorption coefficient. For our particular resonator we have $\lambda \approx 0.94$.

[4] It has been shown that the odd function part is responsible for the generation of odd harmonics and thus for maintaining the oscillation of cylindrical half-open resonators (e.g.[21])

[5] This could be explained with more clearness by using a representation based on the iterative approach as in [20], but that would exceed the scope of this paper

be seen in figure 5 where the amplitude evolutions are shown for $\zeta = \{0.1, 0.2, 0.3\}$ and $\zeta_b = \{0.2, 0.6, 1\}$ and for $\gamma_{(b)}$ values between the oscillation threshold and extinction. We will refer to these curves to discuss the evaluation in the next section.

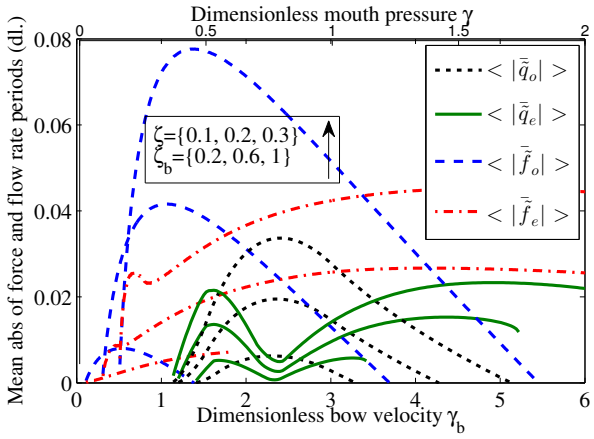

Figure 5: Mean amplitude progressions of the odd and even parts of the SR and BS characteristic nonlinear curves.

4.3. Pitch

While constant excitation parameters result in a sound with a fixed pitch, the resonator's inharmonic modal distribution together with the variation of the mouthpiece pressure spectrum will result in a varying oscillation frequency. Since the inharmonicity of our resonator is found to be positive, we may expect that an increasing brightness imposes an increasing fundamental frequency (see e.g. [21]).

4.4. Odd-even harmonics amplitude ratio

Based on the odd harmonics in the mouth pressure, the remaining even part of the excitation model's function $\tilde{\bar{q}}_e = \frac{\tilde{\bar{q}}(\tilde{p}) + \tilde{\bar{q}}(-\tilde{p})}{2}$ (also shown in figure 3 and 4 for the BS model) will generate even harmonics in the radiated sound, albeit not so loud. After removing the offset (accounting for the mean air flow) from this curve (by subtracting its mean value), just like for the odd function, the "(mean absolute) even amplitude" is calculated $< |\tilde{\bar{q}}_e| >$, whose evolution for the excitation parameter ranges is also shown in figure 5. It is interesting to note that, particularly for the SR case, the even amplitude reaches a minimum where its odd counterpart is maximal. By studying the mean amplitudes of both functions this provides a crude preestimation of what the odd/even harmonics amplitude ratio of the produced sound will be.

5. EVALUATION

Both the SR and BS models were executed with the hybrid instrument as well as with a modal simulation of the resonator with 14 modes[6]. As the resonator simulation is fairly accurate [1, 13] (and the amplifier and microphone responses are reasonably flat), it may be supposed that the shortcomings of the loudspeaker (such as nonlinearities) are the main reason for the difference between hybrid and simulated results. In order to obtain a pressure signal that corresponds to the sound radiated by the instrument, the approximated external pressure can be calculated by $p_{ext} \propto \frac{d(p+q)}{dt}$ (supposing a monopole radiation). To cope with the amplification of high frequency noise, prior to the derivative a steep low-pass filter is applied, with $f_{cutoff} = 4\,\text{kHz}$, at the resonance frequency of the upper simulated mode.

To allow for a quantitative and relevant comparison of hybrid and simulated sounds, we use so-called "sound descriptors". These represent a standardized set of features that describe relational values derived from the spectral, temporal and harmonic representations of the sound. We chose to consider two physically and perceptively relevant descriptors: the "harmonic spectral centroid" (HSC), which can be seen as the spectral gravity centre of the harmonic content and is known to be highly correlated to the brightness of that part of the sound (the normal spectral centroid turned out to be influenced by the raucous sound for the BS case, which we want to ignore for that comparison); and the "odd/even harmonics ratio" (OER), which is the ratio of odd and even harmonic amplitude components[7]. We also studied the mean (RMS) amplitude evolution of the mouthpiece pressure and the progression of the fundamental frequency.

Only the steady state regime is evaluated and the applied parameter values are $\zeta = \{0.1, 0.2, 0.3\}$ and $\zeta_b = \{0.2, 0.6, 1\}$ with $\gamma_{(b)}$ increasing from the oscillation threshold until extinction and $\delta = 0.375$, $\alpha = 0.5$. The relatively low $\zeta_{(b)}$ values are due to parasitic noises with the hybrid instrument. However, for the SR case, ζ still spans about half of the aforementioned typical range, and for the BS case it can be argued that the ζ_b range is reasonable as it is implied that "the string is bowed in the middle". The dynamic parameters for the SR model are held fixed to the values used in [16]: $\omega_r = 2\pi \times 2500\,\text{rad}\,\text{s}^{-1}$ and $Q_r = 5$. This is a relatively high resonance frequency for a fundamental frequency of $f_0 \approx 140\,\text{Hz}$, but that makes the model similar to the more elementary static reed model (we note that an evaluation with $\omega_r = 2\pi \times 10\,\text{krad}\,\text{s}^{-1}$ had virtually the same results). Since the SR case has already been discussed in earlier papers [2, 1], we will mainly consider the BS results and the comparison with the SR results. We note that a higher $\zeta_{(b)}$ implies a wider oscillatory $\gamma_{(b)}$ domain, so that this can be used to identify the $\zeta_{(b)}$ values of the curves in figures 6 to 9.

Figure 6 shows the progressions of the mean (RMS) mouthpiece pressure signals.

The theoretical results are obtained from the intersection of the nonlinear curves that include the frequency independent losses. They are close to the simulated results for low $\gamma_{(b)}$ values, but it should be noted that the theoretical curves represent the peak-to-peak amplitude, so that the decreasing RMS amplitudes may be explained by the reduction of high frequencies. The extinctions (where the RMS amplitudes drop to zero with increasing $\gamma_{(b)}$) coincide fairly well, except for $\zeta_b = 0.6$. Considering the BS's odd amplitude in figure 5, it becomes clear that this is most likely due to the lack of odd harmonics delivered by the BS excitation.

The simulated and hybrid curves for both BS and SR models match closely, apart from the fact that the hybrid extinction occurs slightly earlier, which may be due to the influence of the uncompensated loudspeaker losses. Another important difference occurs for the BS model near to the oscillation threshold: a raucous sound (characteristic to bowed strings) appears, but for the hybrid instrument that state is more prominent and is sustained for much longer, particularly for high bow forces. For

[6] The sounds can be found online on: http://users.mct.open.ac.uk/kb22747/

[7] For the precise mathematical definition of the sound descriptors see [22, 23].

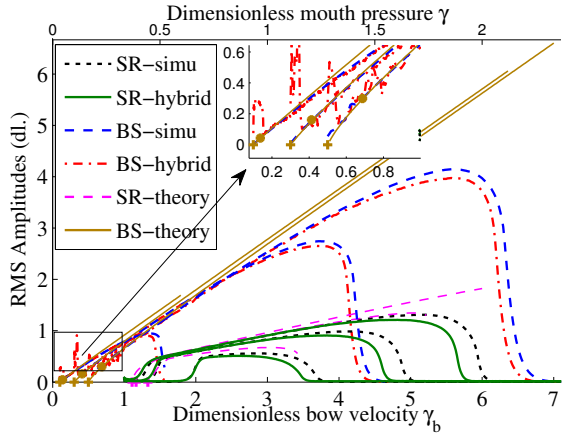

Figure 6: Mean (RMS) amplitude progressions of the pressure at the resonator entrance for the hybrid and simulated results with the SR and BS models, and theoretical SR and BS peak-to-peak amplitudes.

very low bowing velocities, the hybrid instrument produced unstable squeaks (visible as overshooting peaks). We assume that this occurrence, and the generally unstable hybrid behaviour when the nonlinear function contains steep variations (e.g. for $\zeta_{(b)}$ values above the here applied range), is due to the phase lag introduced by the loudspeaker. At high frequencies it can rotate the phase by $180°$ so that the downwards going static friction curve will be converted into a (high) negative resistance which makes the system unstable.

Figure 7 represents the harmonic spectral centroid ("HSC") curves. Comparing these curves with the odd amplitudes in fig-

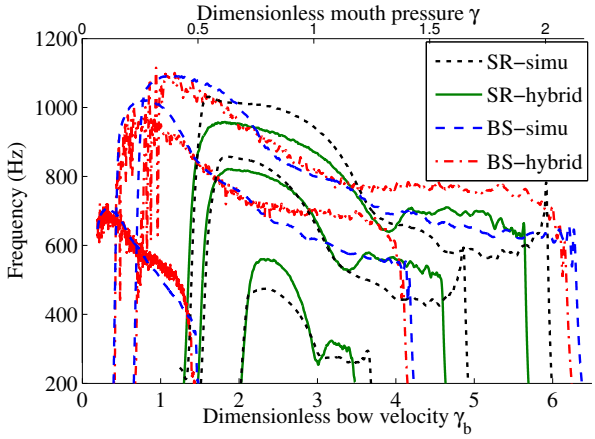

Figure 7: Harmonic spectral centroids for the hybrid and simulated results with the SR and BS model.

ure 5 we find a surprisingly good overall resemblance of the relative progressions where even the interrelation between SR and BS curves is respected to a good extent. It appears that the relationship between the odd amplitude and the HSC is reasonably linear. The simulated and hybrid BS cases correlate with a similarly good precision as for the SR case.
We note that for the case of the SR model, it has been shown that both the spectral centroid and the attack time of a note onset are highly correlated features, which are mainly controlled by the excitation amplitude ζ [22, 2]. This feature is not studied in this paper, but we assume that similar results can be expected for the BS model.

Figure 8 represents the fundamental frequency (f_0) progressions for all cases. As predicted, this feature is well correlated with the spectral centroid due to the positive inharmonicity of the resonator. However, as pointed out earlier, the loudspeaker introduces a phase lag that makes the inharmonicity negative, resulting in an inverse correlation for the hybrid cases. It can further be seen that these hypotheses are supported by the outcome with the BS model.

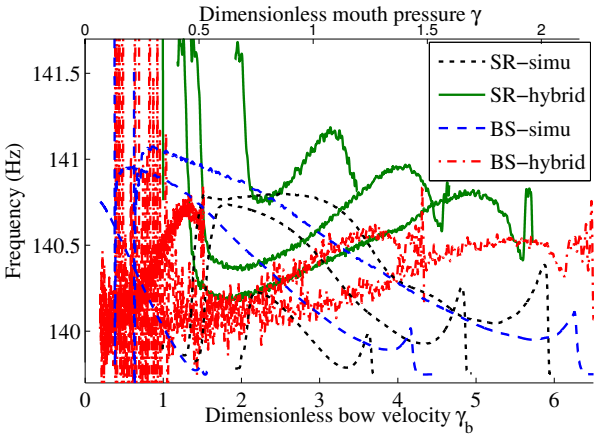

Figure 8: Fundamental frequency progressions for the hybrid and simulated results with the SR and BS model.

Finally, figure 9 depicts the odd/even harmonics amplitude ratio ("OER").

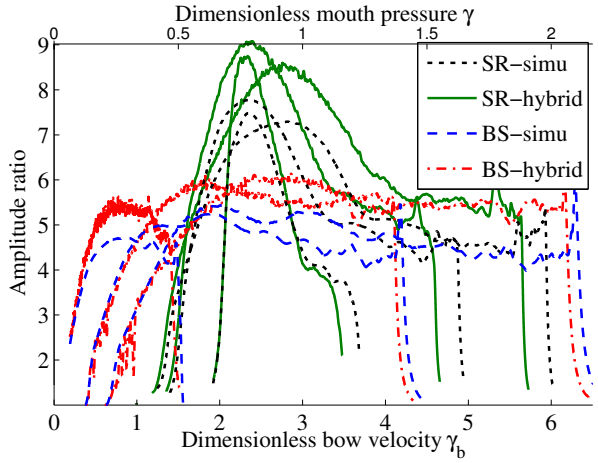

Figure 9: Odd/even harmonics ratio progressions for the hybrid and simulated results with the SR and BS model.

Considering the even amplitudes in figure 5, it can be seen that the OER has important correlations with the ratio of the odd and even amplitudes. For the SR case, the coinciding peak/dip situations in the latter explains the peaks for the OER, while for the BS this is far less the case, resulting in a more moderate OER progression.

6. DISCUSSION AND CONCLUSIONS

After a brief review of the hybrid wind instrument set-up, we presented the classical single-reed (SR) mouthpiece model and

the hyperbolic bow-string (BS) interaction model with absorption of torsional waves. Via analogy with the SR model, a dimensionless and reduced parameter form is proposed for the BS model, which reveals that the SR model's dimensionless mouth pressure γ has an analogous function as the dimensionless bowing speed γ_b. The SR model's "embouchure parameter" ζ is a direct factor to the whole nonlinear function whereas for the BS model, the bow force ζ_b has a similar role but it does not affect the slope of the static friction curve. This shifts the γ_b "oscillation threshold" and "raucous threshold" (as indicated by Schelleng's maximum bowing force [24]) upwards for increasing ζ_b. Solely considering (quasi-)static excitation models (which is sufficient for our study), we derived a graphical method to draw an intuitive link between the characteristic nonlinear curve and a few features of the produced sound: the amplitude of oscillation, the spectral richness and the amount of odd and even harmonics.

Next, the SR and BS excitation models were implemented with both the hybrid wind instrument and a modal simulation of the resonator. The resulting differences can be mainly attributed to uncompensated characteristics of the loudspeaker. For both models, typical parameter values were applied, although the $\zeta_{(b)}$ range had to be constrained to prevent parasitic noises with the hybrid instrument. These are assumed to occur as a result of phase shifts which can exceed 180° at high frequencies, thereby transforming the (higher) positive resistance slope in the nonlinear functions into a negative one, which can cause an instability at those frequencies.

Three $\zeta_{(b)}$ values were applied with an increasing $\gamma_{(b)}$ from oscillation threshold until extinction. The resulting sound features (RMS pressure, harmonic spectral centroid, fundamental frequency and odd/even harmonics amplitude ratio) were found to be well predicted by the graphical method. The hybrid results are in overall good accordance with the simulations and hypotheses related to the loudspeaker are made to explain the differences.

The difference in sound between the SR and BS models is not substantial, except for the (typical) raucous sound appearing with the BS model when γ_b/ζ_b is low. This similarity is potentially a result of the simplifications (static) in both models. An empirical evaluation with more dynamic models (e.g. the "lip-reed" as in brass instruments) resulted in a stronger timbral variation.

7. REFERENCES

[1] K. Buys, D. Sharp, and R. Laney, "Developing a hybrid wind instrument : using a loudspeaker to couple a theoretical exciter to a real resonator," in *Proc. Int. Symp. Music. Acoust.*, 2014.

[2] K. Buys, D. Sharp, and R. Laney, "Developing and evaluating a hybrid wind instrument excited by a loudspeaker," in *Proc. Inst. Acoust.*, 2014, vol. 36.

[3] T. A. Wilson and G. S. Beavers, "Operating modes of the clarinet," *J. Acoust. Soc. Am.*, vol. 56, pp. 653–658, 1974.

[4] C. Maganza, *Excitations non linéaire d'un conduit acoustique cylindrique. Observations de doublements de période précédant un comportant chaotique. Application à la Clarinette*, Ph.D. thesis, Université du Maine, 1985.

[5] J. Guérard, *Modélisation numérique et simulation expérimentale de systèmes acoustiques - Application aux instruments de musique*, Ph.D. thesis, Université Paris 6, 1998.

[6] N. Grand, *Etude du seuil d'oscillation des systèmes acoustiques non-linéaires de type instrument à vent*, Ph.D. thesis, Université Paris 7, 1994.

[7] T. Meurisse, A. Mamou-Mani, R. Caussé, B. Chomette, and D. B. Sharp, "Simulations of Modal Active Control Applied to the Self-Sustained Oscillations of the Clarinet," *Acta Acust. united with Acust.*, vol. 100, no. 6, pp. 1149–1161, 2014.

[8] K. Buys and C. Vergez, "A hybrid reed instrument: an acoustical resonator with a numerically simulated mouthpiece," in *Proc. Acoust. 2012*, Nantes, 2012.

[9] M. E. McIntyre, R. T. Schumacher, and J. Woodhouse, "On the oscillations of musical instruments," *J. Acoust. Soc. Amer.*, vol. 74, no. 5, pp. 1325–1345, 1983.

[10] S. Ollivier, J. P. Dalmont, and J. Kergomard, "Idealized models of reed Woodwinds. Part I: Analogy with the bowed string," *Acta Acust. united with Acust.*, vol. 90, no. 6, pp. 1192–1203, 2004.

[11] G. Weinreich and R. Caussé, "Elementary stability considerations for bowed-string motion," *J. Acoust. Soc. Amer.*, vol. 89, no. 2, pp. 887–895, 1991.

[12] G. Muller and W. Lauterborn, "The Bowed String as a Nonlinear Dynamical System," *Acustica*, vol. 82, no. t 996, pp. 657–664, 1996.

[13] K. Buys, D. B. Sharp, and R. Laney, "Developing and evaluating a hybrid wind instrument," *Acta Acust. united with Acust.*, p. to appear.

[14] "Xenomai: Real-Time Framework for Linux," .

[15] A. Hirschberg, "Aero-acoustics of wind instruments," in *Mech. Music. Instruments*, A. Hirschberg J. Kergomard and G. Weinreich, Eds. Springer, Wien, 1995.

[16] P. Guillemain, J. Kergomard, and T. Voinier, "Real-time synthesis of clarinet-like instruments using digital impedance models," *J. Acoust. Soc. Am.*, vol. 118, no. 1, pp. 483, 2005.

[17] J. H. Smith and J. Woodhouse, "The tribology of rosin," *J. Mech. Phys. Solids*, vol. 48, pp. 1633–1681, 2000.

[18] R. Pitteroff and J. Woodhouse, "Mechanics of the contact area between a violin bow and a string. Part I: Reflection and transmission behaviour," *Acta Acust. united with Acust.*, vol. 84, no. 3, pp. 543–562, 1998.

[19] A. Askenfelt, "Measurement of the bowing parameters in violin playing. II: Bow-bridge distance, dynamic range, and limits of bow force," *J. Acoust. Soc. Amer.*, vol. 86, no. 2, pp. 503–516, 1989.

[20] P.-A. Taillard, J. Kergomard, and F. Laloë, "Iterated maps for clarinet-like systems," *Nonlinear Dyn.*, vol. 62, no. 1-2, pp. 253–271, Dec. 2010.

[21] J. Kergomard, S. Ollivier, and J. Gilbert, "Calculation of the Spectrum of Self-Sustained Oscillators Using a Variable Truncation Method : Application to Cylindrical Reed Instruments," vol. 86, no. June 1999, pp. 685–703, 2000.

[22] M. Barthet, *De l'interprète à l'auditeur : une analyse acoustique et perceptive du timbre musical*, Ph.D. thesis, Université de la Méditerranée Aix-Marseille II, 2009.

[23] G. Peeters, B. L. Giordano, P. Susini, N. Misdariis, and S. McAdams, "The Timbre Toolbox: Extracting audio descriptors from musical signals," *J. Acoust. Soc. Amer.*, vol. 130, no. 5, pp. 2902–2916, Nov. 2011.

[24] J. C. Schelleng, "The bowed string and the player," *J. Acoust. Soc. Am.*, vol. 53, no. 1, pp. 26, 1973.